

Observations and Analysis of Beimen Sandbank Surface Change Using Multi-Temporal UAV Datasets

Ruli Andaru^{1,2} & Jiann-Yeou Rau¹

¹Department of Geomatics, National Cheng Kung University, Tainan City, Taiwan (R.O.C.)

²Department of Geodetic Engineering, Gadjah Mada University, Indonesia

Email: ruliandaru@ugm.ac.id; jyrau@geomatics.ncku.edu.tw

KEYWORDS: Sandbank, change analysis, multi-temporal, UAV, photogrammetry

ABSTRACT: Understanding topographic change of sandbank is important in order to monitor ecological function and sustainability of human life along the seashore area. This paper presents the study on topographic change analysis at Beimen sandbank by using multi-temporal UAV (unmanned aerial vehicle) imagery. Due to the Beimen's coastline morphology over large spatial scales (4 km alongshore, i.e., approximately 4 km² of sand-dune system), we use a VTOL (Vertical Take Off and Landing) UAV to acquire high spatial resolution images. In order to reveal the sandbank topographical changes, we used five time series data acquired between February and July of year 2019 and propose a novel strategy to co-register multi-temporal datasets. After dense image matching, we found corrupted pointclouds with significant amount of noise and outlier in the water surface due to image matching failed. To overcome it, we apply Random Forest-Machine Learning (RFML) for removing these outliers in unordered pointclouds. This approach is efficient and robust to remove amounts of noise and outliers, especially in the water surface with sun reflection and wave, while being able to handle large and dense sampled pointclouds. According to its result, we generate DSM from the refined pointclouds and analyze the erosion and accumulation effects at Beimen's sandbank area. Finally, we calculate the erosion and accumulation volume and identify the area affected by erosion and accumulation. We noticed that the highest accumulation area occurs between May 19th and July 4th, with an estimated accumulation area of 1,111,282.20 m² and accumulation volume of 224,549.60 m³ due to the heaviest rainfall occurred at July 2nd and 3rd. Furthermore, we obtained a total of erosion area with 934,497.60 m² between July 4th and July 17th.

1. INTRODUCTION

Beimen sandbank is located at the western of Jing Zai Jjiao Salt Field, Beimen District, Taiwan. As shown in Figure 1, it has 4.2 km length along the west coast and has important function for sustainable human life at the seashore area. Sandbank surface, therefore, is very complex and the topological changes are dynamic due to natural coastal factors, i.e. ocean wave, tidal forces, wind, rainfall and typhoons. In addition, the spatial change of sandbank surface is important to monitor ecological function at the sandbank area. To accomplish it, we use multi-temporal UAV imagery to monitor its land cover and topographical changes. To figure out the spatial change of the sandbank, five time series data were acquired, i.e. Feb 23rd, April 20th, May 19th, July 4th and July 17th by using a VTOL type UAV, named Saber A.



Figure 1. Beimen sandbank at western Taiwan seashore.

Photogrammetric techniques had been successfully applied to detect and monitor large-scale coastal dune change of Truc Vert beach which was representative open sandy beaches of the 110km long Gironde coast in France (Fauret, et al., 2019). In addition, UAV platform had successfully performed and represented a promising technique for high resolution reconstruction of topography on coastal environments at Ravenna, Italy (Mancini, et al., 2013). Furthermore, UAV had already been successfully exploited to monitor the topography of dynamic tidal inlet (Long, et al., 2016) and calculate sand volume (Yoo & Oh, 2016) on the south-east coast of Korea.

The important issue while we use multi-temporal UAV datasets in sand area is co-registration among those data since there is no ground control points (GCP) on the sandbank area. Moreover, because the sea shore contains large area of waterbody, not only ocean but also fish ponds, corrupted pointclouds will appear with significant of noise and

outlier in the water surface due to image matching failed. This research mainly focus on two topics. Firstly, we propose a strategy to co-register multi-temporal UAV images with no GCP at the sandbank area. The second one is to analyse sandbank surface change and identify the erosion and accumulation area affected by heavy rainfall.

2. DATA AND METHODS

2.1 UAV & images data collection

In this study we collect data in two regions, i.e., sandbank and inland area (Figure 2). Since we are not able to acquire the GPS field measurement of GCPs at the sandbank area (red region), but we can survey GCPs at the inland area (green region), we need to conduct several UAV flights at the inland area and process it together with the one at the sandbank area. There are 3 flight strips which contain 6 flight lines at the inland area, i.e., B1, B2, B3 and we named it as “base frame”. We also use “base frame” UAV images to conduct on-the-job self-calibration. Meanwhile, in the sandbank area we only acquire only one strip, which contains 2 flight lines, and we carry out five epochs in 2019, i.e. T1 (Feb 23rd), T2 (April 20th), T3 (May 19th), T4 (July 4th), and T5 (July 17th).



A. BASE REGION (Inland area)

STRIP LINE	B1			B2		B3
Year	2019					
UAV type	Unmanned VTOL (Vertical Take Off and Landing) type					
Date	2019-05-19	2019-05-24	2019-07-17	2019-05-19	2019-05-24	2019-05-19
Altitude (m)	400	400	300	400	300	400
Images #	1022	859	1036	1056	1052	1120

B. SANDBANK AREA

EPOCH TIME	T1		T2	T3	T4	T5
Year	2019					
UAV type	Unmanned VTOL (Vertical Take Off and Landing) type					
Date	2019-02-23	2019-02-24	2019-04-20	2019-05-19	2019-07-04	2019-07-17
Altitude (m)	400	400	400	400	400	400
Images #	476	554	1471	1118	913	1033
GSD (cm)	11.1	11.1	11.1	11.1	11.1	11.1

Figure 2. Two area of UAV’s data collection and image database

To acquire the aerial images, we use a Saber A-VTOL UAV as shown in Figure 3. The advantage of VTOL UAV is that it can take off and landing vertically, like a multi-rotary UAV, but acquire imagery like a fixed-wing UAV. Using the 6 cells 25000 mAh battery, it is capable to fly 80km of traveling distance which is suitable for large area or corridor mapping, like the sandbank area. This UAV carries Sony A7r2 with 15mm focal length lens. With a flying altitude of 400m, it can produce high resolution orthoimage with a GSD (Ground Sampling Distance) of 12cm and build DSM (Digital Surface Model) in 0.5m GSD.



Figure 3. UAV Saber A-VTOL

2.2 The proposed strategy

There are two issues regarding to surface change analysis at the sandbank area by using multi-temporal UAV image. The first one is the way to co-register all datasets, i.e. pointclouds, DSM, ortho-image, accurately, particularly at the sandbank area where has no GCPs. All of GCPs are located at the inland area, as shown in Figure 4, so that we need to co-register the time series of sandbank images with inland images. To cope with this problem, we simulate two co-registration strategies during aerial triangulation of images (Rau, et al., 2019). The first one is “independent method”, meaning that we fix the EOPs of the “base frame” images when conduct aerial triangulation with each epoch’s UAV images, i.e. no tie-point among the all epochs of images. The second one is the “combined method” by combining the “base frame” images with all epochs’ UAV images (Figure 5) during aerial triangulation. In which, the “base

frame” images should be calibrated in advance by a rigorous aerial triangulation (AT) procedure. The EOPs of “base frame” images are fixed while performing AT with sandbank images. By using this configuration, the camera’s position and orientation of Base Frame images will not move or changed, thus it will force the time series images (T1-T6) connected to the “base frame” tightly and co-register the produced pointclouds accurately.

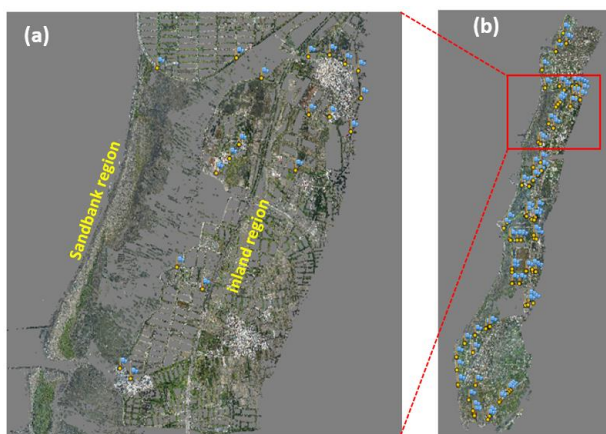


Figure 4. GCPs (blue flags) distribution.
(a) Beimen seashore area, (b) The whole Tainan seashore.

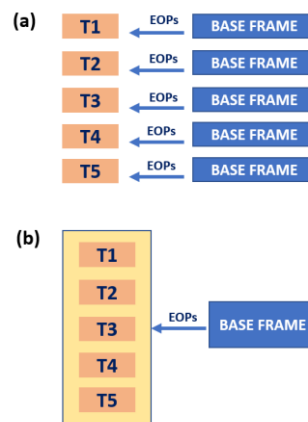


Figure 5. Two strategy of co-registration (AT) process. (a) independent AT, (b) combined AT

The second issue is noisy pointclouds in the waterbody due to image matching failure. To cope with this issue, we adopt Random Forest Machine Learning (RFML) method provided by Lidar 360 software to extract the noisy points and remove them automatically. The method could handle unstructured and inhomogeneous pointclouds with strong variations in point density (Hackel, et al., 2016).

2.3 Methodology of analyses surface change

To calculate the difference between two datasets, we apply cloud to cloud comparison (C2C) algorithm provided by Cloud Compare software to compute the discrepancy between two time-series pointclouds. The cloud-to-cloud distance apparently indicates the surface change of sandbank between two time series datasets. Based on pointclouds data, we generate DSM and analyze the erosion effect occurred at Beimen’s sandbank at the common zone. The common zone is defined by intersection of 0m elevation contour lines on five epoch time as shown in Figure 6.

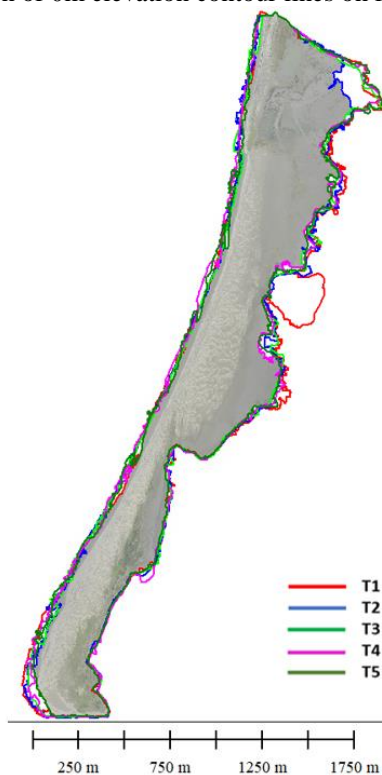


Figure 6. Common area at the sandbank area, defined by intersection of 0m contour line from all time-series data

We also analyse the surface changes by comparing the DSM and surface profiles to identify the erosion and accumulation area. Furthermore, we calculate the erosion and accumulation volume of sandbank at the common zone and use 0 m elevation as reference (Figure 7).

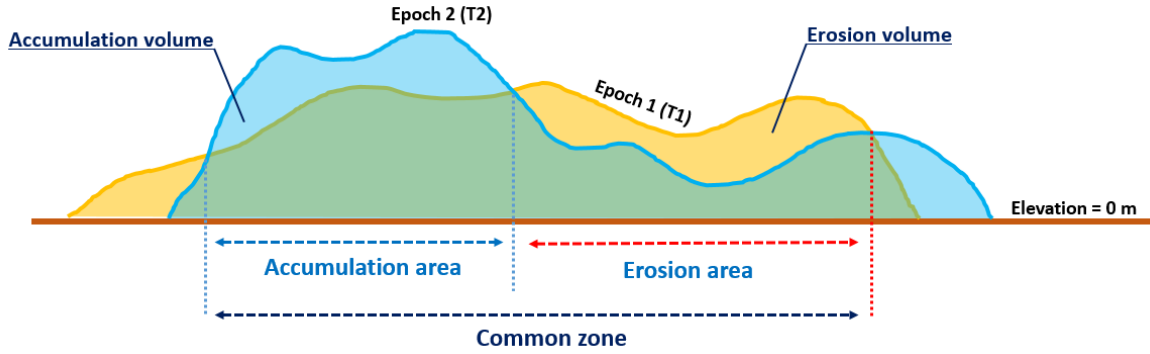


Figure 7. Surface change analysis between time-series T1 and T2.

3. RESULTS AND DISCUSSION

3.1 UAV image triangulation accuracy analysis

In this study, we observe 30km long and 1km width seashore along Taiwan western coast as shown in Figure 4(b). In total, there are 96 control/check points surveyed by eGNSS method. We conduct AT using Agisoft Metashape software. During AT bundle adjustment, some of them are marked as GCPs and the others are treated as ICPs (independent check points). The algorithms detect and match the feature points in different camera perspectives by using Scale Invariant Feature Transform (SIFT) algorithms (Carrivick, et al., 2016). Then, it reconstruct 3D scene structure through SfM(Structure from Motion) technique as well as solving the interior and exterior orientation parameters (IOPs/EOPs) of the camera and images. For rigorous and accurate AT purpose, we apply gradual filtering by removing tie-points that were matched from a minimum number of images together with a small reprojection error. The statistics of AT accuracy analysis results are shown in Table 1. The RMS of GCP and ICP for all cases are smaller than 20 cm and the overall reprojection error is roughly around 1 pixel. This proves that both strategies are accurate, reliable and stable.

Table 1. Statistics of AT accuracy

Co-registration Strategy	Independent					Combined
	T1+Base	T2+Base	T3+Base	T4+Base	T5+Base	(T1+T2+T3+T4+T5)+ Base
Images #	6085	6386	6049	5833	6047	10178
Altitude	445	444	439	439	438	451
GSD (cm)	13	12.9	12.8	12.8	12.7	13.1
GCP RMS xy (cm)	14.08	13.42	15.42	14.31	14.74	13.07
GCP RMS z (cm)	13.4	13.42	16.18	13.76	13.33	15.76
ICP RMS xy (cm)	16.45	16.22	17.28	16.74	16.77	16.15
ICP RMS z (cm)	15.35	16.22	15.97	15.41	15.1	16.15
Reprojection error (pixel)	0.97	0.93	1	0.99	0.98	0.97
GCP/ICP #	42/48	46/50	46/50	43/48	46/50	46/50

3.2. Co-registration of multi-temporal datasets

Both co-registration strategies show that the AT results are accurate. However, in order to prove that all time series images have been well co-registered, we should check the surface profiles of all epochs at non-changed objects, e.g. building and road. Furthermore, we also check the number of valid tie-point matched between neighborhood images. The higher the valid tie-point is, the better the co-registration results. Figure 8 shows the surface profile comparison of both strategies. According to this figure, we notice that co-registration using “independent” strategy has high elevation difference and inconsistency profiles among all five time series datasets. Moreover, it has fewer number of valid tie-point compared with the “combined” strategy. Two tie-point matching examples are shown in Figure 9, in which the blue lines denote valid matching, while the red lines denote invalid one between neighborhood images. Although the number of valid tie-point matching does not increase considerably, it still improves the consistency of surface profiles significantly in the whole time series data. Base on this comparison, we notice that “combined” strategy is better to co-register multi-temporal datasets than the “independent” one.

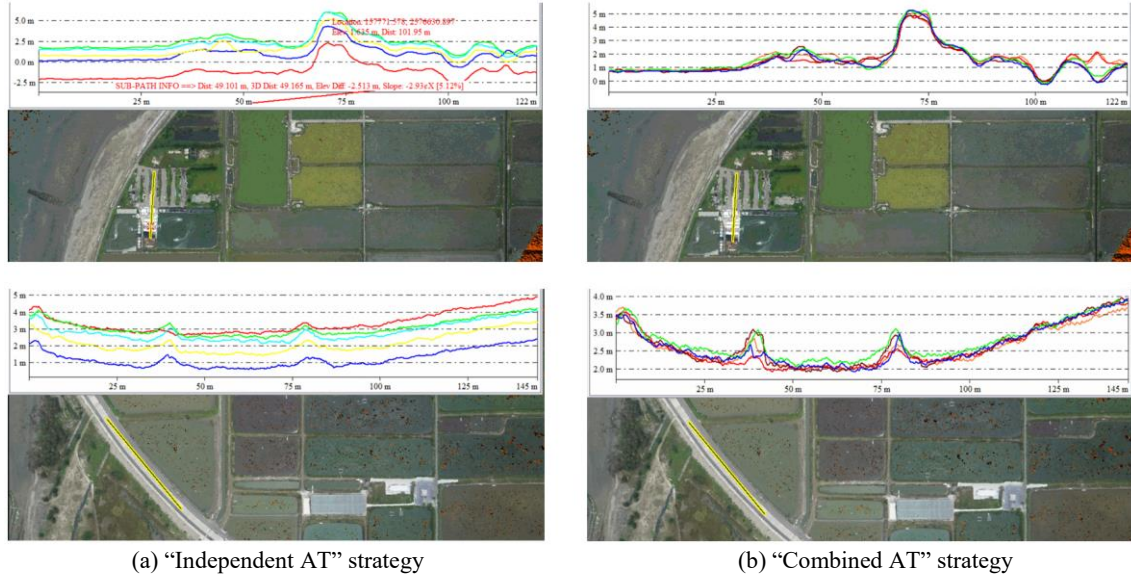


Figure 8. Surface profiles comparisons, in which different colors denote different epochs.

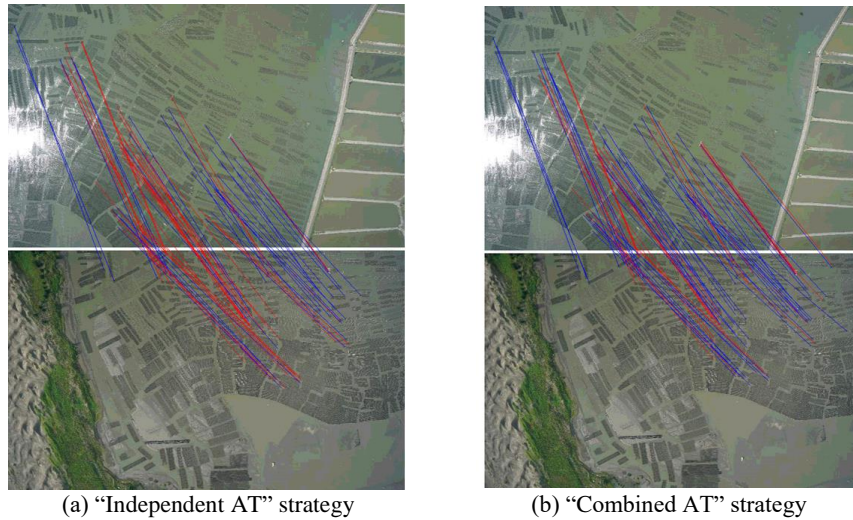


Figure 9. Tie-points matching results between neighbored images.

3.3. Noise removal on water surface

After performing AT process, we generate 3D dense pointcloud using Multi View Stereo (MVS) dense image matching algorithm, and then produce DSM and orthophoto of sandbank area. Due to image matching failure on the water surface area, it contains a huge noise and outlier pointclouds as shown in Figure 10(a) and 10(c). To overcome it, we apply RFML algorithm to remove the outliers. Random Forests are the combination of tree predictors such that each tree depends on the values of a random vector sampled in-dependently and with the same distribution for all trees in the forest (Breiman, 2001). It provides an accurate classification and run on large datasets efficiently, also measures the variable importance for each class. The feature selection is obtained by backward elimination of features depending on their importance (Chehata, et al., 2009).

There are 3 main steps while use RFML to remove noisy pointclouds, i.e. create and define the training data, generate trained model and classifying the data (Green-Valley, 2018). The machine learning classification use the trained model for determining individual point classifications based on a statistical model of user-defined feature types. They have a good predictive performance even when most predictive variables are noisy. In this study, Random Forests were successfully applied to classify unstructured and inhomogeneous pointclouds derived from photogrammetric reconstruction, especially in the water surface with sun reflection and wave. After the model has trained, a large amount of data is processed in batch, and it is therefore reduce the amount of labor significantly. We classify and separate the pointclouds into four classes, i.e. noisy, ground surface, vegetation and buildings. For producing refined pointclouds, we merge all pointclouds classes but exclude noisy points. Figure 10(d) shows the refined pointclouds after RFML noise removal and Figure 10(b) shows the DSM generated from the refined pointclouds.

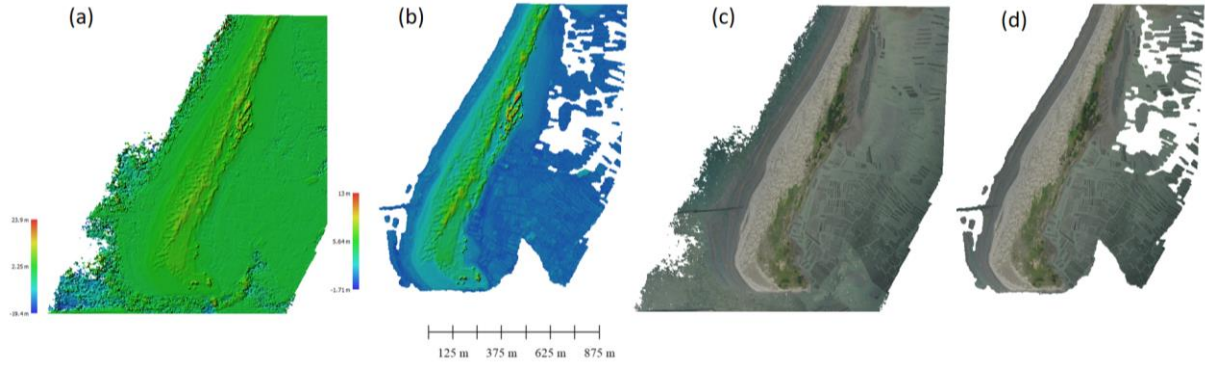


Figure 10. Before and after noisy removal by using RFML algorithm

3.4. Pointclouds and surface change analysis

Through photogrammetric and machine learning processes we have obtained refined 3D pointclouds at the sandbank area for all five epochs. For topographic change analysis, we eliminate the pointclouds below an elevation reference, i.e. 0m. Figure 11 shows the remaining pointclouds above 0m elevation.

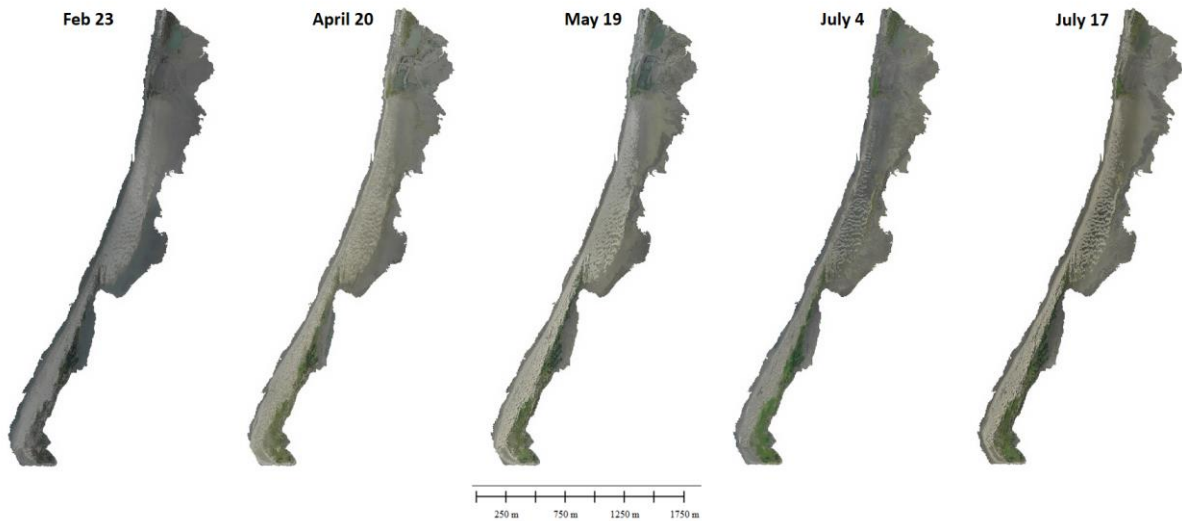
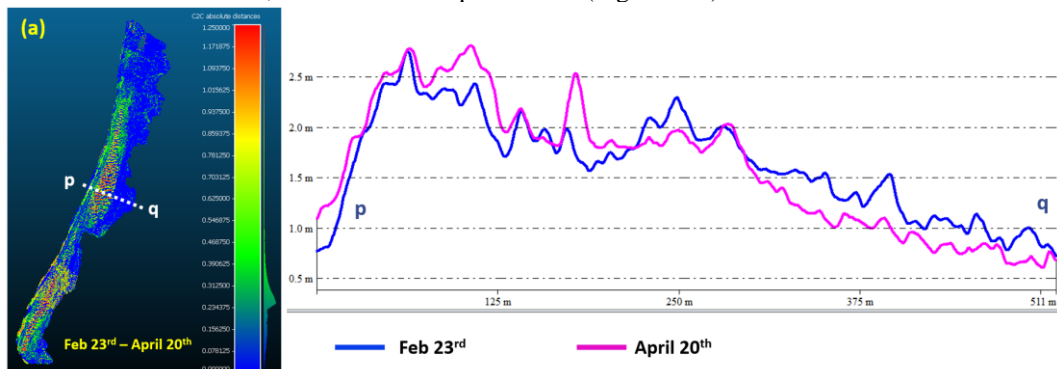


Figure 11. Pointclouds above 0m elevation reference

We also calculate the distance on consecutive time series data to understand their surface changes at the common area. Figure 12 shows the pseudo coloured images according to the scalar field on C2C algorithms and the surface profile based on the DSM data. The red color indicates maximum distance value, whereas the blue one has the lowest distance. Since C2C shows in absolute distance, we use cross section profile in order to identify the height difference and quantify the changes of elevation between two surfaces. Based on cloud distance we found a significant change occurs between February 23rd (T1) and April 20th (T2) as indicates in red color. From the surface profile, in the line p-q, we observe that the elevation difference around 0.8m as shown in Figure 12a. Furthermore, we found that the highest accumulation change occurs between May 19th and July 4th with elevation difference around 0.4m, as shown in line profile t-u (Figure 12c). We also found the highest erosion change occurs between July 4th and July 17th with elevation difference around 0.3m, as shown in line profile v-w (Figure 12d).



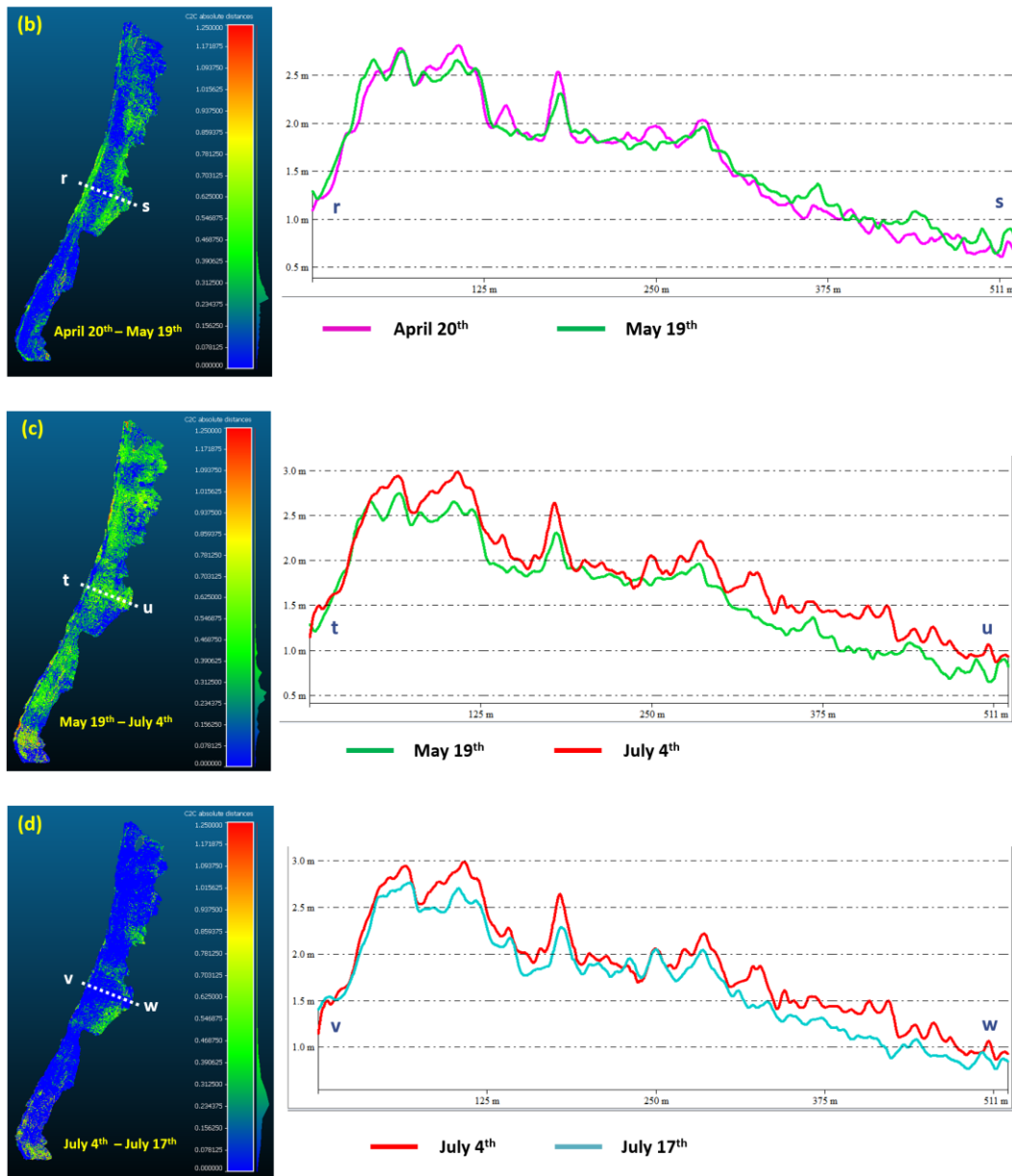


Figure 12. Pseudo coloured images according to the scalar field and the surface profile between each time-series data.

3.5. Erosion and accumulation area of sandbank

We also calculate erosion and accumulation area within the common zone on consecutive time series data. The erosion area occurs when waves and currents remove sand from the beach. The loss of sand causes the beach to be narrower and lower in elevation (USGS, 2016). Figure 13 shows the erosion as indicated in red color, whereas the accumulation area is indicated in blue color. The highest accumulation area occurs between May 19th and July 4th, indicated by the dominance of blue color covering in almost surfaces of the sandbank, with an estimated accumulation area of 1,111,282.2 m². Meanwhile, the highest erosion area occurs between July 4th and July 17th with an estimated erosion area of 934,497.6 m². It happens due to the lowest precipitation in Beimen area at July 12nd until 16th, i.e. 3.16 mm (CWB, 2019) The erosion and accumulation area on consecutive time series data are illustrated in Table 2.

Table 2. Erosion and accumulation area

Epoch	Date		Duration (day)	Horizontal Movement	
	Start	End		Erosion area (m ²)	Accumulation area (m ²)
T1-T2	2019-02-23	2019-04-20	56	676,874.20	641,091.20
T2-T3	2019-04-20	2019-05-19	29	83,935.40	781,835.00
T3-T4	2019-05-19	2019-07-04	46	249,269.90	1,111,282.20
T4-T5	2019-07-04	2019-07-17	13	934,497.60	417,297.00

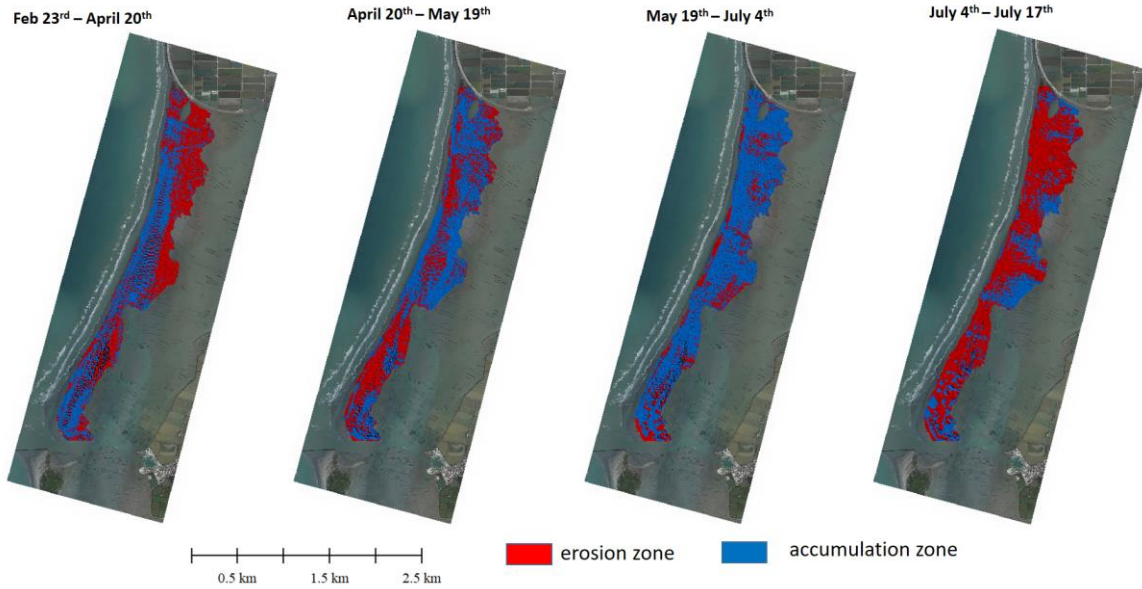


Figure 13. The erosion and accumulation area.

3.6. Erosion and accumulation volume

To demonstrate the sandbank volume change, we generate DSM elevation difference on consecutive time series data. It further provides quantitative information of change in elevation and the erosion or accumulation volume at the sandbank as shown in Figure 14. The green-red color indicates sand erosion and blue-yellow color indicates sand accumulation. By understanding this result, we notice that the significant change occurs between May 19th (T3) and July 17th (T4) as shown in Figure 14, corresponding to the results of the accumulation volume as illustrated on Table 3, i.e. 224,549.60 m³. It happens due to the largest precipitation in Beimen area at July 2nd until 3rd, i.e., 113.5 mm (CWB, 2019). Heavy rainfall really affects landscape changes and surface elevation around the sandbank area. This phenomenon will retreat the sand back to the ocean and accumulation to the inland area.

Table 3. Volume calculation between each time series data

Epoch	Date		Duration (day)	Volume Change	
	Start	End		Erosion Volume (m ³)	Accumulation Volume (m ³)
T1-T2	2019-02-23	2019-04-20	56	115,317.20	139,716.60
T2-T3	2019-04-20	2019-05-19	29	67,928.20	121,235.30
T3-T4	2019-05-19	2019-07-04	46	37,017.70	224,549.60
T4-T5	2019-07-04	2019-07-17	13	170,763.60	58,756.50

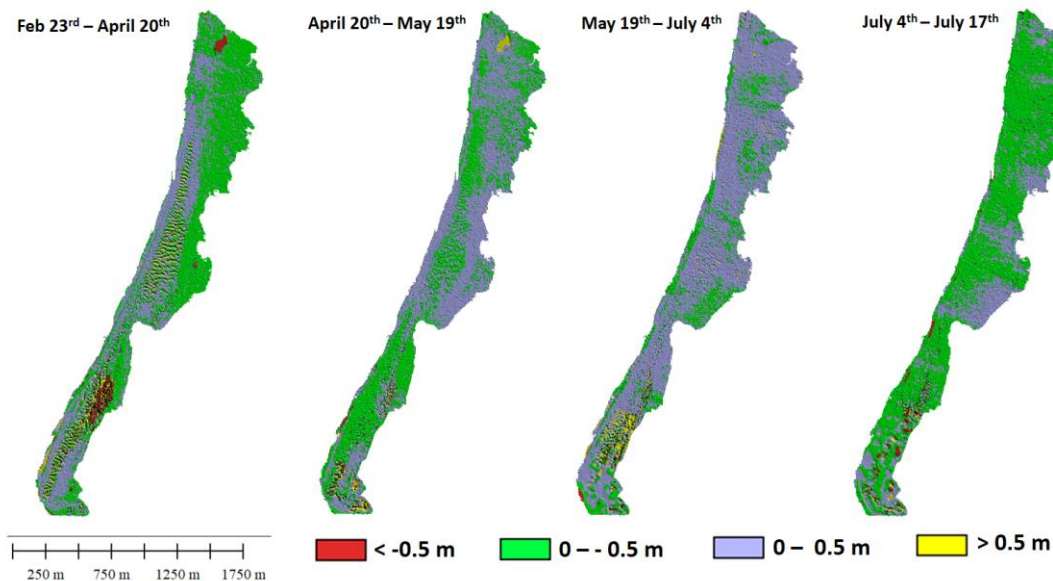


Figure 14. DSM elevation difference between each dataset

4. CONCLUSIONS

In this study, we adopt UAV photogrammetry and spatial analysis to monitor topographic changes in the sandbank area. UAV have attracted a lot of attention in the field of remote sensing, since they present advantages of ubiquitous usability, flexible deployment, high maneuverability, multi-sensory, and provide a cost-effective service with acceptable accuracy. To monitor topographic sandbank changes, we conduct multi-temporal image acquisition during the lowest tidal time, which is more flexible by utilizing UAV as platform. However, since west Taiwan's sand-dune morphology over large spatial scales, i.e. 30 km alongshore corridor area and with no control point at the sandbank surface, it causes a weak imaging geometry. The other problem is the way to co-register the entire time series datasets. To accomplish it, we propose two strategies to co-register multi-temporal UAV images in the sandbank area, i.e. "independent" and "combined" aerial triangulation strategies. According to the AT accuracy results, we have observed 0.987 pixel of reprojection error and less than 20cm of GCP/ICP RMS error. However, from the DSM elevation differences and the number of valid tie-point matching, we have proven that the "combined AT" strategy for co-registration is more accurate and consistent for five time series datasets.

Through photogrammetric and machine learning processing, we have obtained a refined 3D pointclouds at the sandbank area and calculate their distance on consecutive time series datasets to better understand the surface changes. We also calculate erosion and accumulation area in the common area through 0m contour lines. The highest accumulation area occurs between May 19th and July 4th had an accumulation area of 1,111,282.20 m² and accumulation volume of 224,549.60 m³. For erosion area, we have obtained the highest erosion area occurs between July 4th and July 17th with erosion area of 934,497.60 m².

Base on the results, we concluded that photogrammetric pointclouds and DSM generated from UAV imagery can perform periodical surface change monitoring. Moreover, we can measure not only their erosion and accumulation area but also volumetric changes. It is useful to monitor its dynamic changes for the purpose to maintain the functionality of the sandbank.

5. REFERENCES

- Breiman, L., 2001. *Random Forests*. s.l.:Statistics Department, University of California Berkeley, CA 94720.
- Carrivick, J.L., Smith, M.W., Quincey, D.J., 2016. *Structure from Motion in the Geosciences*. s.l.:John Wiley & Sons, Ltd, United Kingdom.
- Chehata, N., Guo, L. & Mallet, C., 2009. *Airborne Lidar Feature Selection for Urban Classification Using Random Forests*. s.l., IAPRS, Vol. XXXVIII, Part 3/W8.
- CWB, 2019. *Taiwan Central Weather Bureau*. [Online] Available at: <https://www.cwb.gov.tw/V7e/climate/dailyPrecipitation/dP.htm> . [Accessed 02 08 2019].
- Fauret, Q. I. et al., 2019. Low-Cost UAV for High-Resolution and Large-Scale Coastal Dune Change Monitoring Using Photogrammetry. *Journal of Marine Science and Engineering*, Volume J. Mar. Sci. Eng. 2019, 7, 63; doi:10.3390/jmse7030063.
- Green-Valley, 2018. *LiDAR 360 User Guide*.
- Hackel, T., Wegner, J. D. & Schindler, K., 2016. *Fast Semantic Segmentation of 3D Point Clouds with Strongly Varying Density*. s.l., ISPRS Annals of Photogrammetry Remote Sensing and Spatial Information Sciences III-3, 177-184.
- Liu, J.-K. et al., 2008. *The Geomorphometry of Rainfall-Induced Landslides in Alishan Area Obtained by Airborne Lidar and Digital Photography*. Boston, IEEE Xplore, pp. 1220-1223.
- Long, N. et al., 2016. Monitoring the Topography of a Dynamic Tidal Inlet Using UAV Imagery. *Journal Remote Sensing*, Volume Remote Sens. 2016, 8, 387; doi:10.3390/rs8050387.
- Mancini, F. et al., 2013. Using Unmanned Aerial Vehicles (UAV) for High-Resolution Reconstruction of Topography: The Structure from Motion Approach on Coastal Environments. *Remote Sensing Journal*, Volume Remote Sens. 2013, 5 .
- Rau, J.-Y., Jhan, J. P. & Andaru, R., 2019. *Landslide Deformation Monitoring by Three-Camera Imaging System*. s.l., <https://doi.org/10.5194/isprs-archives-XLII-2-W13-559-2019>.
- USGS, 2016. *Coastal Change Hazards: Hurricanes and Extreme Storms*. [Online] Available at: <https://coastal.er.usgs.gov/hurricanes/coastal-change/beach-erosion.php#>. [Accessed 20 08 2019].
- Yoo, C. & Oh, T., 2016. *Beach Volume Change using UAV Photogrammetry Songjung Beach*. s.l., The International Archives of the Photogrammetry, Remote Sensing and Spatial Information Sciences, Volume XLI-B8, 2016.